

Variable Stiffness Fiber with Self-Healing Capability

Alice Tonazzini, Stefano Mintchev, Bryan Schubert, Barbara Mazzolai,
Jun Shintake, and Dario Floreano*

Soft hardware technologies^[1] are increasingly used in structures, actuators, and robots intended for unstructured environments,^[2] user safety,^[3] and tasks requiring high dexterity or conformability such as manipulation,^[4–6] locomotion,^[7] rehabilitation, and surgical operations.^[8] However, material compliance, a distinctive feature of soft technologies, can become a limiting factor for situations that require exertion or withstanding of substantial forces. For example, inherently soft mobile robots are advantageous for their robustness and ability to squeeze into small breaches and to change shape according to the locomotion mode or task;^[7] however, sustaining their own weight, carrying significant loads, or exerting high contact forces for fast movement remains a challenge. Similarly, soft endoscopes can advance by adapting to the tortuous paths in the human body and thus minimizing pain and damage to the surrounding tissues, but stiffness is instrumental to performing surgical operations, such as biopsies.^[9] Soft technologies can also be useful for rehabilitation devices that adapt to different body parts and morphologies, but these devices require some degree of stiffness in order to transmit precise forces to accurately assist movement of the desired body part^[10] or sustain the weight of injured body parts. Another challenge is the control of entirely soft systems because they can have multiple, possibly infinite, active degrees of freedom (DoFs); the conventional approach to control DoFs in soft robotics consists of using a single actuator for each active DoF, but this has the drawback of making the system complex, bulky, and thus difficult to miniaturize.^[11]

To address the above-mentioned limitations, materials with controllable stiffness have been integrated in soft structures.^[12–14] Under certain stimuli those materials can selectively tune the load-bearing capabilities of the bodies where they are embedded according to the intended use;^[12] also they can enhance the hosting structures' controllability by selectively

stiffening or locking DoF and therefore achieving complex configurations and motion patterns with a reduced number of actuators.^[13] For example, wax was recently used to create composites that are thermally tunable between few KPa and 1 MPa.^[14] Electro rheological (ER) and magneto rheological (MR) fluids,^[13,15] which, respectively, respond to high electric or magnetic fields by changing their viscosity, have been widely used in damping mechanisms for the automotive industry^[16] and for human prostheses,^[17] in clutches, brakes,^[18] and valves;^[13] however, their low yield stress and the need of additional rigid hardware, such as electromagnets or high voltage capacitors (activation), have limited their further integration into other applications.^[19] Shape memory polymers (SMP)^[19] and conductive elastomers^[20] display moderate (KPa) to high (MPa) stiffness states, but have relatively long response times caused by poor thermal conductivity.^[21] Low melting point alloys (LMPA) are metal alloys that become liquid at relatively low temperatures (47–62 °C, depending on the alloy composition). In the solid state, they have relatively high stiffnesses; for example, the field metal alloy has a stiffness of more than 3 GPa, which is several times higher than all of the above cited materials.^[21–23] Furthermore, an LMPA maintains its solid, load-bearing state without energy consumption, in contrast to ER and MR fluids. External or direct heating can be used to melt the LMPA.^[24,25] Its thermal conductivity is one or more orders of magnitude higher than wax and SMP^[21] and results in a faster phase change and therefore response time. Recently, the outstanding features of LMPAs have been exploited in the form of multi-layered composites,^[24] metallic microstructures embedded in soft elastomers,^[25] and metal–elastomer foams.^[26] For example, the latter can become 20–30 times softer, 200 times more deformable, and it can self-heal when the internal metallic mesh is melted by an external heat source, although large structures raise the issue of melting the entire volume (e.g., a $27 \times 27 \times 9 \text{ mm}^3$ cuboid required 500 °C air blow for almost 80 s).^[26]

Here we propose a fast-switching, variable stiffness fiber (VSF) with embedded heater, composed of an LMPA core, a tubular encapsulation made of silicone rubber, and a helical conductive wire used as a heater for melting the alloy (Figure 1A). The fiber can become >700 times softer and >400 times more deformable when heated above the LMPA melting temperature (62 °C); furthermore, it can be knotted, knitted, clamped, or bonded and it can be fabricated with diameters of few millimeters and lengths of several meters. This versatility facilitates its integration with other components and structures (e.g., fabric^[27]) and their optimization for specific functions or loading conditions. The fiber has self-healing capabilities and high deformability when in the soft state (Figure 1B,C) and a high load-bearing performance

Dr. A. Tonazzini, Dr. S. Mintchev, Dr. B. Schubert,
Dr. J. Shintake, Prof. D. Floreano
Laboratory of Intelligent Systems
École Polytechnique Fédérale de Lausanne
Lausanne 1015, Switzerland
E-mail: dario.floreano@epfl.ch

Dr. B. Mazzolai
Center for Micro-BioRobotics
Istituto Italiano di Tecnologia
Pontedera 56025, Italy

This is an open access article under the terms of the Creative Commons Attribution-NonCommercial-NoDerivatives License, which permits use and distribution in any medium, provided the original work is properly cited, the use is non-commercial and no modifications or adaptations are made.

DOI: 10.1002/adma.201602580



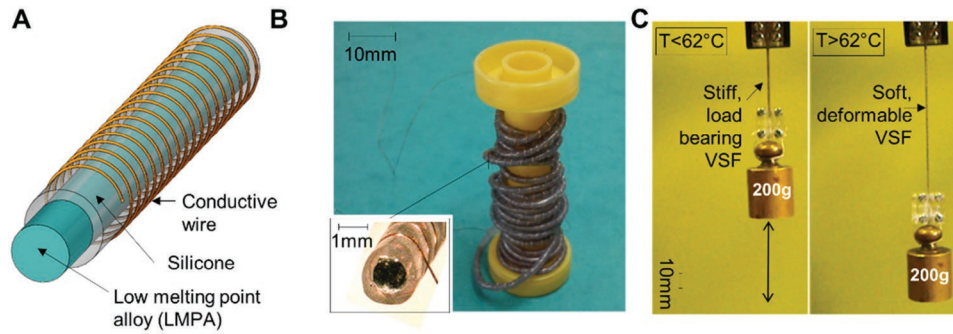


Figure 1. Variable stiffness fiber (VSF) based on low melting point alloy (LMPA). A) Schematic representation of the three VSF components: LMPA core (radius r , length L), silicone encapsulation (total radius R), and conductive wire (radius r_{wire} , length L_{wire}). B) VSF of 550 mm length and total radius of 1.03 mm, wrapped around a spool; in the corner, a picture of the cross section of VSF is shown. C) VSF loaded with a 200 g load. Left: in solid state the VSF ($r = 0.54$ mm, $L = 40$ mm, $R = 1.03$ mm) sustains the load; right: when current is injected into the external heater and the temperature exceeds 62 °C, the VSF softens and deforms under the load.

when in the stiff state (Figure 1C). To support these claims, we describe the use of VSF in three different applications, each selected to address a specific limitation of purely soft technologies: (1) a robot capable of morphing to serve different uses and locomotion modes, (2) two wearable devices for rehabilitation of injured fingers, and (3) a soft pneumatic actuator with a single pressure chamber and multiple controllable DoFs.

The VSF has two states (stiff and soft), which correspond to two physical LMPA phases (solid and liquid). The LMPA core (field metal, HiTech Alloys, WA, USA) is encapsulated by a thin silicone layer (platinum cured silicone tube, Silex LTD, UK) and heated by a conductive wire, which is helically wrapped outside the silicone (Figure 1A). When current is applied to the heater, the temperature of the LMPA core increases due to the conductive transfer of the Joule heating released by the heater. When the LMPA melting temperature ($T_m = 62$ °C) is reached,

the LMPA core transitions from solid (stiff) to liquid state (soft) (Text S1, Supporting information).

In the soft state, the VSF exhibits high strain and low stiffness (Movie S1, Supporting Information and Figure 1C), like a silicone tube filled with liquid. In the stiff state, the VSF behaves like a metal wire (Movie S1, Supporting Information) and is capable of carrying both compressive and tensile loads (Figure 1C).

The VSF can be easily manufactured by sucking molten LMPA into commercial silicone tubes (Materials and Methods, Supporting Information and Figure 2); then, the helical conductive wire is wrapped around the tube. The fabrication process adds self-healing properties to the VSF by pre-stretching the silicone tube (Figure 2, step 2) to pressurize the LMPA in the liquid phase (Figure 2, step 4). Any fracture in the LMPA core in the solid state is self-repaired thanks to the internal pressure that rejoins the two sides of the fracture and fusion bonding that

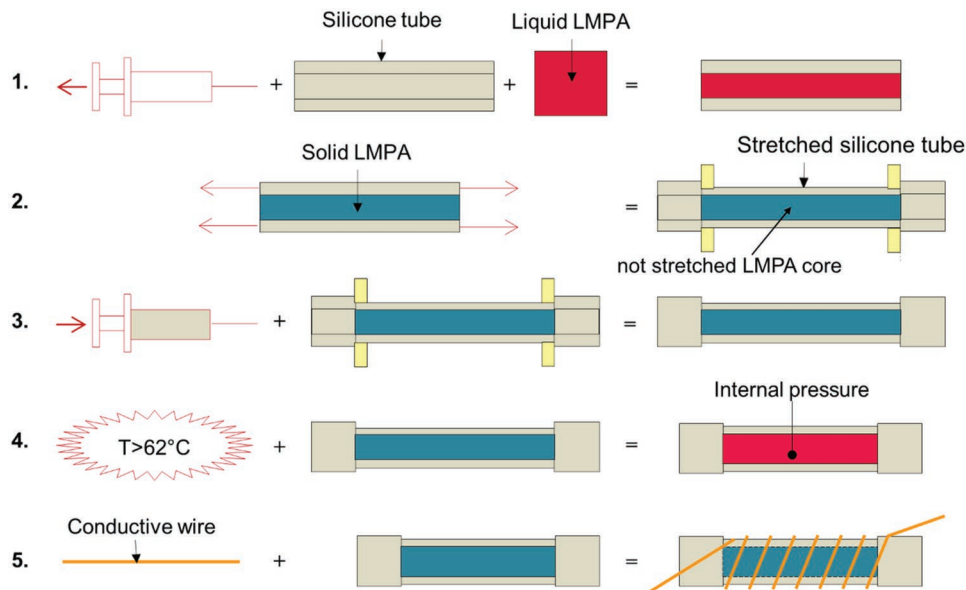


Figure 2. VSF fabrication process. In steps 2 and 3 the pre-stretching of silicone tube is maintained through clamps (in yellow). See also Materials and Methods in the Supporting Information.

occurs when the fiber is heated (Movie S2, Supporting Information). Without any pre-stretching or mechanical stimulation, this healing process is hampered by interface phenomena (e.g., oxidation, wettability) of the liquid alloy,^[25] which prevent re-soldering between the fractured surfaces.^[26]

The final dimensions of VSF and its overall mechanical properties and self-healing capabilities can be controlled during manufacturing: they are function of the initial geometry, elastic properties, and pre-stretching of the silicone tube (see Materials and Methods and Figure S2A–C, Supporting Information).

In order to quantify the VSF mechanical properties, tensile tests were performed on VSFs characterized by different diameters of LMPA core and pre-stretching $\epsilon_0 = 25\%$ (namely, the series: 0.25rp, 0.5rp, 0.75rp, Table S2, Materials and Methods, and Figure S3, Supporting Information).

In the soft state, the LMPA core is liquid and the VSF can deform more than 400% (0.5rp series, Figure 3A). The corresponding ultimate tensile strength is 2.13 ± 0.50 (SD) MPa

(0.5rp series, Figure 3A). The stress–strain curve of VSF is characteristic of elastomers;^[8] it is linear up to $\approx 20\%$ strain (Figure 3A, and Figure S4, Supporting Information). Moreover, the effect of the strain rate on the VSF stress–strain curve is not significant (range of strain rate applied: $0.009\text{--}0.9\text{ s}^{-1}$, Figure S4, Supporting Information).

In ref. [25] the authors described the Young's modulus of an LMPA–elastomer composite through a model of composite material mechanics.^[28] According to that, the liquid alloy behaves as an empty space and the Young's modulus $E_{\text{VSF}}^{\text{soft}}$ of the VSF in the soft state can be calculated as a percent of the Young's modulus E_{SIL} of silicone as follows

$$E_{\text{VSF}}^{\text{soft}} = E_{\text{SIL}} \frac{A_{\text{SIL}}}{A_{\text{TOT}}} \quad (1)$$

where A_{SIL} is the cross-sectional area of silicone and A_{TOT} is the total cross-sectional area of the VSF.

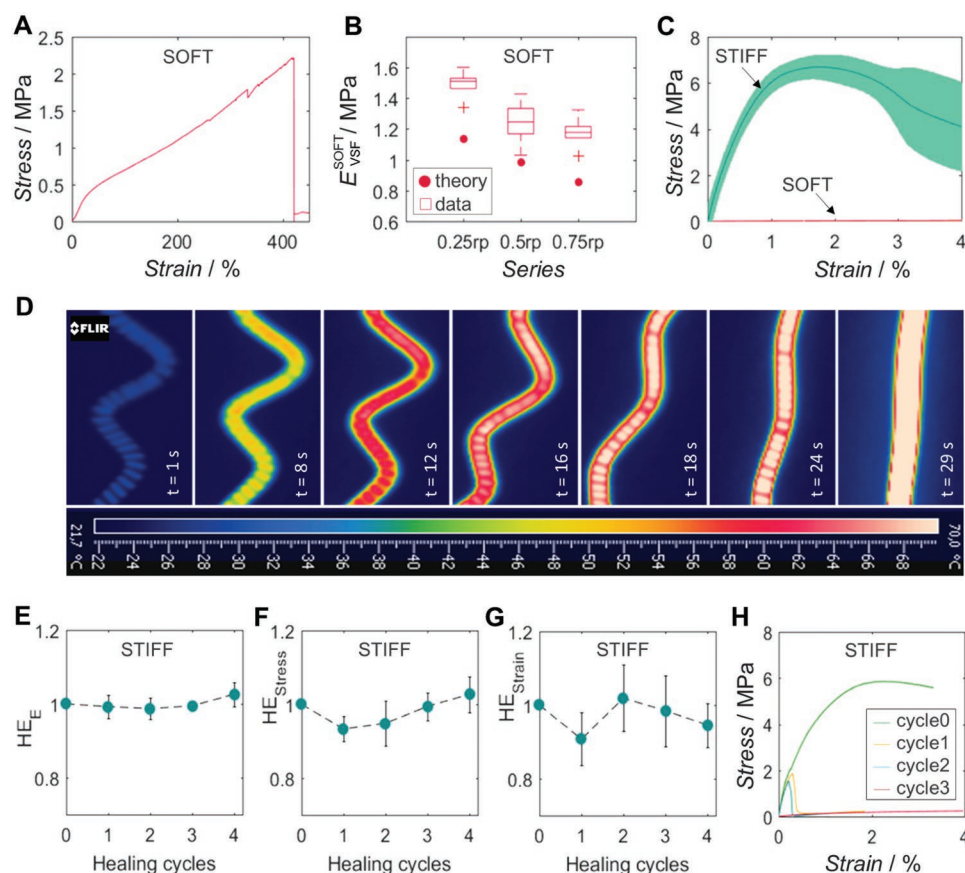


Figure 3. Characterization of the mechanical performance of VSFs (series 0.25rp, 0.5rp, 0.75rp, Table S2, Supporting Information) in the soft and in the stiff state, shape recovery, and self-healing. A) Representative stress–strain curve for VSF (series 0.5rp) in the soft state, deformed up to rupture. B) Young's moduli of VSFs in the soft state (series 0.25rp, 0.5rp, 0.75rp). The plot was made with the MATLAB Boxplot function using default parameters. C) Mean stress–strain curves for VSF series 0.5rp in soft and stiff state. Error bars are the standard deviation of the mean (n tests = 3 for each state). D) Thermal camera pictures (FLIR Systems, Inc., Sweden) of a VSF (series 0.5rp, length $L = 130$ mm) that recovers its original straight shape during the transition from stiff to soft state, starting from a serpentine-shaped configuration. The VSF was heated up by a copper wire (radius $r_{\text{wire}} = 0.04$ mm, length $L_{\text{wire}} = 600$ mm), where a 1.1 A current was injected. The heater was turned on at $t = 0$ s. E–G) Healing efficiency indexes related to Young's modulus, ultimate tensile strength, and corresponding deformation for VSFs series 0.5rp in the stiff state, subjected to consecutive healing cycles. Error bars represent the standard error of the mean. H) Stress–strain curves of a representative not pre-stretched VSF (0.5rp) when subjected to consecutive tensile tests (and to corresponding following melt-and-cool cycles).

In accordance to Equation (1), VSFs with increasing diameters of LMPA cores displayed Young's moduli $E_{\text{VSF}}^{\text{soft}}$ decreasing from 1.49 ± 0.09 (SD) MPa for the 0.25rp series to 1.18 ± 0.09 (SD) MPa for the 0.75rp series (Figure 3B). The theory slightly underestimates the experimental data (Figure 3B): the liquid LMPA core is an incompressible fluid under pressure (Figure 2) and under constant volume conditions, which increases the VSF axial stiffness, as previously shown in ref. [29].

If stretched when in the stiff state, VSFs exhibit ductile failure where the LMPA core necks down before fracture (Figure 3C). In Figure 3C, the VSF (series 0.5rp) reaches the ultimate tensile strength 6.89 ± 0.39 (SD) MPa when its LMPA core necks, for a corresponding deformation of $1.83\% \pm 0.20$ (SD). The resulting Young's modulus $E_{\text{VSF}}^{\text{stiff}} = 887.79 \pm 55.69$ (SD) MPa is more than 700 times higher than in soft state.

The LMPA core plays the main role in sustaining the imposed deformation when solid, while the silicone encapsulation gives a negligible contribution to the overall performance. Indeed, when the mechanical properties are calculated by considering the initial cross-sectional area A_{LMPA} of the LMPA core (rather than the total cross-sectional area A_{TOT} of the fiber), the resulting values of the Young's modulus (3229 ± 202 (SD) MPa), ultimate tensile strength (3229 ± 202 (SD) MPa), and the corresponding deformation (1.83 ± 0.20 (SD) %) are not significantly different with respect to the values measured in the LMPA alone (Wilcoxon rank sum test, p -values $P = 0.40$, $P = 0.63$, $P = 0.40$, respectively).

If a strain is imposed when VSF is soft (e.g., stretching, bending, see Text S2 and Figure S6, Supporting Information), the radius of the LMPA core may vary: this fact influences the structural functionality of the VSF, once cooled down in the deformed shape.

While the VSF is studied here either in soft or rigid state, LMPA stiffness can also be controlled to intermediate values;^[25] however, in that case precise temperature control is required because the change of stiffness occurs within a narrow range of temperatures.^[25] The melting temperature is the main parameter that drives the choice of a specific LMPA (e.g., Cerrolow 117 (HiTech Alloys) melts at 47°C); this temperature depends on the composition of the alloy that, in turn, determines the mechanical properties of the material. Furthermore, the VSF could also use other types of melting materials, such as thermoplastic materials (e.g., PCL^[30]) offering a wider range of temperature for finer tuning of intermediate stiffness values, however at the cost of a reduced stiffness change.

After extreme deformations, including those causing fracture of the solid LMPA core, the VSF recovers its original shape and functionality after a melt-and-cool cycle thanks to the already mentioned self-healing capability (Movie S2, Supporting Information).

Figure 3D shows the shape recovery process of a VSF without loads: the shape recovery is driven by the elastic force of the pre-stretched silicone encapsulation. During melting, both the liquid and the solid phase coexist in the LMPA core. Full shape recovery occurs when the entire volume of the LMPA core is liquid (Text S1 and Figure S5, Supporting Information).

Furthermore, reheating and cooling a deformed or broken fiber also restores its mechanical properties in the solid state: Young's modulus, ultimate tensile strength, and strain. These

properties were measured on VSFs after consecutive healing cycles (cycles 1–4) and compared to the corresponding original values (before onset of healing cycles, cycle 0): no significant differences exist (Wilcoxon signed rank test, no significant differences, $P > 0.25$ in all the cases) (Tables S3–S5, Supporting Information). The healing efficiency of each mechanical property (Young's modulus, ultimate tensile strength, and strain), which is the ratio between its value measured after each consecutive healing cycle and the original one, was unitary and constant across multiple cycles and different VSF diameters (Figure 3E–G for the VSF series 0.5rp). Furthermore, 80% of consecutive tensile tests on the same VSF resulted in core LMPA fractures occurring at different locations, which suggests that the self-healing process does not leave localized defects in the LMPA core, excluding pre-existing air bubbles due to the fabrication.

When subjected to consecutive cycles, an un-pre-stretched VSF tends to fracture in the same location (90% of trials) and its ultimate tensile stress and strain decrease across cycles (0.5r in Figure 3H). After a certain number of cycles (typically less than 3), the heating process is not sufficient to guarantee even a partial re-bonding of LMPA core surfaces (Figure 3H). This result highlights the importance of the internal pressure in the liquid alloy created by the pre-stretching during fabrication for obtaining self-healing.

While in the soft state, the VSF can be morphed into different shapes that are preserved after cooling (shape fixity). This capability can be useful to change the shape of robots that are expected to display multiple functionalities.^[31] For example, we have used VSF in the four arms of an H-shaped robot that can fly like a hovering drone, move on the ground like a wheeled vehicle, and fold around its core for storage or transportation (Figure 4A, and Movie S3, Supporting Information). The frame has four arms made of VSF, each equipped with an electric motor and a foldable propeller (Text S3 and Figure S7, Supporting Information). The four arms can take different functional morphologies: (1) deployed in a quadrotor-like configuration (Figure 4A on the left) with high bending stiffness to withstand propeller thrust and ensure stability during flight, (2) bent toward the ground in a four-wheeled configuration (Figure 4A in the center) for terrestrial locomotion where the folded propellers operate like wheels, and (3) folded around its core in a stowed configuration for ease of storage and transportation (Figure 4A on the right). Furthermore, the self-healing capability of VSF makes the platform resilient against collisions. If an arm fractures or bends after a collision and loses rigidity or shape, a simple reheating makes the vehicle capable of flying or rolling again.

The low temperature phase shift, high stiffness, and deformation range make VSF a promising solution to the conflicting requirements—strength versus adaptability—of wearable rehabilitation devices. A rehabilitation process often requires alternating periods of immobilization and movement during the slow restoration of natural form and function of the musculoskeletal or neuromuscular system. Ideally, the rehabilitation device, such as a splint or cast, should adapt to the changing requirements of the rehabilitation schedule.^[32]

For example, an adaptive splint for an injured finger could be fabricated by clamping two VSFs to two 3D-printed plastic

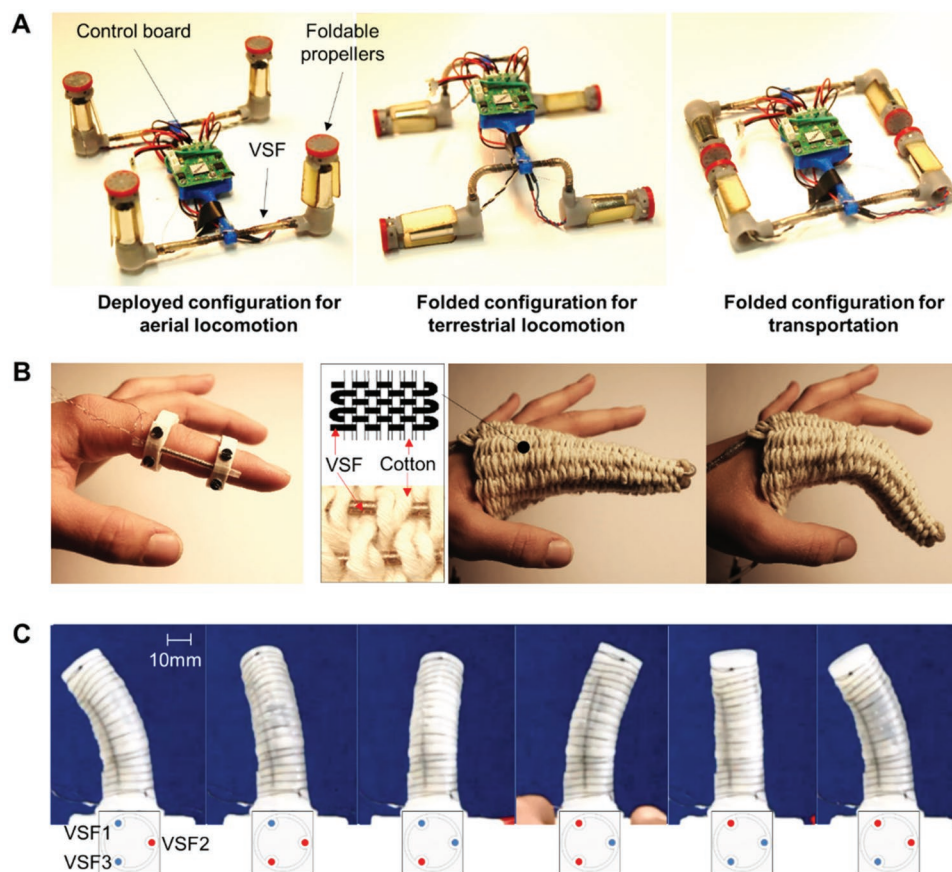


Figure 4. Potential applications of VSF in the fields of morphing systems, wearable rehabilitation, and soft fluidic actuation. A) Views of the foldable multimodal quadrotor with VSF based arms (series 0.75rp, length $L = 30$ mm) in three different configurations: on the left, fly configuration, with deployed arms ($95 \times 95 \times 50$ mm); in the center, folded configuration for terrestrial locomotion; on the right, planar configuration for easy storage and safe transportability ($95 \times 95 \times 20$ mm). B) On the left, prototype of VSF-based finger splint in extended configurations. On the right, prototype of VSF-based cast, obtained by a fabric composed of woven VSF (as warp thread) and cotton filament (as weft thread); the weight of the device is 29 g. In both prototypes, the VSFs (series 0.75rp, length $L = 30$ and 400 mm, respectively) were realized with Cerrow 117 (HiTech Alloys, melting temperature 47°C , see^[25] for other material properties). C) Lateral view of the soft fluidic actuator (external diameter 20 mm, total length 50 mm) with three VSF parts (0.25rp, length $L = 30$ mm) embedded into walls. In the white box, a schematic of the actuator cross section is shown where the state of VSFs is indicated. VSF 1 and VSF 2 are not visible.

rings (Figure 4B on the left and Movie S4, Supporting Information). In the stiff state the splint provides structural support to the injured articulation. When the position of the articulation needs to be modified during rehabilitation, the VSF can be heated to become soft and follow the finger movements without the need for removing the device. If a new fixed position has to be adopted (e.g., extension or bending of the interphalangeal joint in Figure 4B), the VSF can be deformed while soft and keep the new desired configuration after cooling.

The VSF can also be knitted together with a cotton thread to form a criss-cross pattern (“plain weave”) (Figure 4B on the right and Figure S8, Supporting Information). In the soft state, the fabric is extensible and conformable while in the stiff state it is rigid and keeps the shape adopted in the previous phase. This fabric could be used as a wearable cast for bone injuries (Figure 4B on the right and Movie S5, Supporting Information): it can adapt to different anatomies and sizes and, once solid, it can immobilize the area during the healing process. In addition, it is breathable, more hygienic, and faster than conventional plaster (e.g., synthetic cast materials need a curing

time of more than 30 min^[33]). The load-bearing capability of the fabric can be increased either by using a larger LMPA core as long as the total mass of the tissue is comfortable (see Text S4, Supporting Information) or by different knitting patterns and mesh sizes that result in higher direction-specific rigidity. For wearable devices that may be in contact with skin, sweat, and water, the VSF can be fabricated with an internal helical conductive wire, inserted into the silicone pipe before the suction of the melted alloy (Materials and Methods, Supporting Information).

Classical fluidic actuators can bend in multiple directions by selectively pressurizing multiple internal chambers through independent inlet pipes and valves.^[34–36] Such fluidic circuits can be significantly simplified by using a single inflatable chamber whose walls are lined with a number of equidistant VSFs (Figure 4C, and Figure S9 and Movies S6 and S7, Supporting Information). In order to avoid radial expansion of the chamber under pressure, a cotton fiber is wound around the chamber to provide radial reinforcement. This simplified flwc actuator can bend in multiple directions by selectively softening

the VSFs through the Joule heating released by the VSFs' heaters (Figure 4C, and Movie S6, Supporting Information). When the chamber is inflated, the VSF functions as a fixed-length cable that prevents the elongation of the corresponding side of the actuator. If all VSFs are in the stiff state, the chamber is inextensible. If current is supplied to one of the VSFs, the fiber softens and elongates while the pressurized soft body bends in the opposite direction. Once stiffened after deformation, VSFs maintain the actual configuration of the actuator (i.e., bended or elongated) and sustain external loads (shape fixity) (Movie S7, Supporting Information). By increasing the number of VSFs into the actuator structure, it is possible to increase the number of bending directions (i.e., DoF) and improve the shape fixity performance (Movie S7, Supporting Information). The VSFs can be either integrated into the elastomeric walls during the actuator's fabrication (Figure S9, Supporting Information) or glued externally on the already fabricated actuator. Compared to a traditional tri-partitioned fluidic actuator of the same size, this VSF-controlled actuator has a simpler and more compact structure and achieves higher torques.

This new VSF displays remarkable stiffness and elongation range changes (both on the order of a hundred times) coupled with self-healing capabilities that make it reliable and durable. Furthermore, the possibility to embed it into different materials and its low-temperature phase shift also make it suitable for multiple applications ranging from robotics to wearable devices. If integrated into soft bodies, VSFs in the soft state follow the deformation of the host structure with negligible effect on the overall mechanical performance while, in the stiff state, providing high stability and rigidity (e.g., during force exertion by end effectors in soft robots); moreover, VSFs can enclose and protect delicate components (e.g., human body in case of impacts). If used in conventional rigid structures, VSFs enable reconfigurability and morphing ability (e.g., wings of an aerial vehicle).^[29,37]

The VSF fabrication method involves commercially available materials and a simple manufacturing process that allows easy and inexpensive production of several-meter long fibers, which can be cut into the appropriate size for the desired application.

It may be possible to envision alternative ways to melt the core alloy by using an encapsulation layer made of conductive rubber that also serves as a heater; moreover, the integration of particles or fibers in the LMPA may further increase the stiffness variation of the VSF. In the future, an ambitious goal would be to transform the VSF in a stand-alone "robotic material,"^[38] which fully integrates sensing, actuation, and control to mimic the multi-functionality and adaptability of biological systems to their environment. For example, a VSF coupled with fluidic or other smart actuators (e.g., shape memory alloys, dielectric elastomers) could result in an autonomously morphing robot. Taking inspiration from biology, VSFs in inflatable structures (i.e., artificial cells) could play the role of load-bearing micro-fibrils in the real cell wall, whose loosening or stiffening determines the final shape of the cell.^[39,40] On a larger scale, structures that integrate VSF could control load distribution^[38] by localized stiffness change, as human bones and trees do.^[41,42] This could be useful for the development of robust structures ranging from adaptive seating to corrective cloths and orthopedic corsets.

Supporting Information

Supporting Information is available from the Wiley Online Library or from the author.

Acknowledgements

This work was supported by the Swiss National Science Foundation through the National Center of Competence in Research (NCCR) Robotics and by the PLANTOID European project (EU-FP7-FETOpen Grant No. 29343).

Received: May 15, 2016

Revised: August 26, 2016

Published online: September 30, 2016

- [1] D. Rus, M. T. Tolley, *Nature* **2015**, 521, 467.
- [2] D. Trivedi, C. D. Rahn, W. N. Kier, I. D. Walker, *Appl. Bionics Biomech.* **2008**, 5, 99.
- [3] S. Xu, Y. Zhang, L. Ji, K. E. Mathewson, K. Jan, J. Kim, H. Fu, X. Huang, P. Chava, R. Wan, S. Bhole, L. Wang, Y. Na, Y. Guan, M. Flavin, Z. Han, Y. Huang, J. A. Rogers, *Science* **2014**, 344, 70.
- [4] R. Deimel, O. Brock, *Int. J. Robot. Res.* **2016**, 35, 161.
- [5] J. Shintake, S. Rosset, B. E. Schubert, D. Floreano, H. Shea, *Adv. Mater.* **2016**, 28, 231.
- [6] F. Ilievski, A. D. Mazzeo, R. F. Shepherd, X. Chen, G. M. Whitesides, *Angew. Chem.* **2011**, 50, 1890.
- [7] R. F. Shepherd, F. Ilievsky, W. Choi, S. A. Morin, A. A. Stokes, A. D. Mazzeo, X. Chen, M. Wang, G. M. Whitesides, *Proc. Natl. Acad. Sci. USA* **2011**, 108, 20400.
- [8] T. Ranzani, G. Gerboni, M. Cianchetti, A. Menciassi, *Bioinspiration Biomimetics* **2015**, 10, 035008.
- [9] A. Loeve, P. Breedveld, J. Dankelman, *IEEE Pulse* **2010**, 1, 26.
- [10] Y. L. Park, J. Santos, K. G. Galloway, E. C. Goldfield, R. J. Wood, presented at *IEEE Int. Conf. Robotics and Automation*, Hong Kong, China, May **2014**.
- [11] C. D. Onal, D. Rus, presented at *IEEE RAS/EMBS Int. Conf. Biomedical Robotics and Biomechatronics*, Rome, Italy, June **2012**.
- [12] K. Takashima, J. Rossiter, T. Mukai, *Sens. Actuators, A* **2010**, 164, 116.
- [13] A. Sadeghi, L. Beccai, B. Mazzolai, presented at *Int. Conf. Intelligent Robots and Systems*, Vilamoura, Portugal, October **2012**.
- [14] N. G. Cheng, A. Gopinath, L. Wang, K. Iagnemma, A. E. Hosoi, *Macromol. Mater. Eng.* **2014**, 299, 1279.
- [15] C. Majidi, R. J. Wood, *Appl. Phys. Lett.* **2010**, 97, 164104.
- [16] A. Gokhan, X. Wang, F. Gordaninejad, *Smart Mater. Struct.* **2010**, 19, 065024.
- [17] J. H. Kim, J. H. Oh, presented at *IEEE International Conference on Robotics and Automation*, Seoul, Korea, May **2001**.
- [18] C. Rossa, A. Jaegy, A. Micaelli, J. Lozada, *Smart Mater. Struct.* **2014**, 23, 025028.
- [19] K. Takashima, T. Noritsugu, J. Rossiter, S. Guo, T. Mukai, *J. Robot. Mechatron.* **2012**, 24, 472.
- [20] W. Shan, S. Diller, A. Tutcuoglu, C. Majidi, *Smart Mater. Struct.* **2015**, 24, 065001.
- [21] C. Liu, H. Qin, P. T. Mather, *J. Mater. Chem.* **2007**, 17, 1543.
- [22] M. E. Hossain, C. Ketata, M. R. Islam, presented at *Int. Conf. Modeling, Simulation and Applied Optimization*, Sharjah, UAE, January **2009**.
- [23] N. C. Rosenfield, N. M. Wereley, *Smart Mater. Struct.* **2004**, 13, 1303.
- [24] W. Shan, T. Lu, C. Majidi, *Smart Mater. Struct.* **2013**, 22, 085005.
- [25] B. E. Schubert, D. Floreano, *RSC Adv.* **2013**, 3, 24671.

- [26] I. M. Van Meerbeek, B. C. Mac Murray, J. W. Kim, S. S. Robinson, P. X. Zou, M. N. Silberstein, R. F. Shepherd, *Adv. Mater.*, **28**, 2801.
- [27] M. C. S. Yuen, R. A. Bilodeau, R. Kramer, *IEEE Robot. Autom. Lett.* **2016**, *1*, 708.
- [28] R. F. Gibson, *Principles of Composite Material Mechanics*, CRC Press, Boca Raton, FL, USA **1994**.
- [29] Y. Shan, M. P. Philen, A. Lofti, S. Li, C. E. Bakis, C. D. Rahn, K. W. Wang, *J. Intell. Mater. Syst. Struct.* **2009**, *20*, 443.
- [30] M. A. McEvoy, N. Correll, *Compos. Sci. Technol.* **2015**, *49*, 1799.
- [31] L. Daler, S. Mintchev, C. Stefanini, D. Floreano, *Bioinspirations Biomimetics* **2015**, *10*, 016005.
- [32] W. Frontera, *IEEE Eng. Med. Biol. Mag.* **2003**, *22*, 25.
- [33] S. V. Deshpande, *Injury* **2005**, *36*, 1067.
- [34] D. Rus, M. T. Tolley, *Nature* **2015**, *521*, 467.
- [35] K. Suzumori, S. Iikura, H. Tanaka, *IEEE Control Syst. Mag.* **1992**, *12*, 21.
- [36] K. Suzumori, S. Kanda, N. Kato, H. Suzuki, presented at *IEEE Int. Conf. Robotics and Automation*, Rome, Italy, April **2007**.
- [37] W. Wang, H. Rodrigue, S. H. Ahn, *Sci. Rep.* **2016**, *6*, 20869.
- [38] M. A. McEvoy, N. Correll, *Science* **2015**, *347*, 1261689.
- [39] A. Kasprowicz, M. Smolarkiewicz, M. Wierzchowiecka, M. Michalak, P. Wojtaszek, *Mechanical Integration of Plant Cells and Plants*, Springer, Berlin, Germany **2011**, pp. 1–25.
- [40] I. S. Wallace, C. T. Anderson, *Front. Plant Sci.* **2012**, *3*, 1.
- [41] M. A. Meyers, P. Y. Chen, A. Y. M. Lin, Y. Seki, *Prog. Mater. Sci.* **2008**, *53*, 1.
- [42] B. Moulia, C. Coutand, J. L. Julien, *Front. Plant Sci.* **2015**, *6*, 1.